

APPLICATION OF A MATHEMATICAL MODEL TO THE ANALYSIS OF THE INFLUENCE OF LENGTH AND DIAMETER ON LOG DRYING RATE

Maurice Defo

Research Scientist
Centre de Recherche sur le Bois
Département des sciences du bois et de la forêt
Université Laval
Québec, Qc, Canada, G1K 7P4

and

Gilles Brunette

Manager
Composite Wood Products Department
Forintek Canada Corp., Eastern Division
319 rue Franquet
Sainte-Foy, Québec, Canada G1P 4R4

(Received September 2005)

ABSTRACT

A mathematical model based on the water potential concept was used to simulate the effect of length and diameter on the drying rate of aspen logs. The moisture content-water potential relationship and the effective water conductivity were determined during independent experiments. The set of equations describing heat and mass transfer during the drying process were solved by the finite element method. As expected, diameters and lengths had a strong effect on log drying rate. Smaller diameter logs dried faster than larger ones. Shorter logs dried faster than longer ones. Over a critical diameter or length value, however, there was no further marked difference in drying rate for larger or longer logs. For a given length, drying was predominantly radial in smaller diameter logs, whereas in larger logs, longitudinal drying was predominant. For longer logs, drying occurred essentially in the radial direction.

Keywords: Wood yard, log drying model, diameter and length effects.

INTRODUCTION

It is common practice in the composite wood panel industry to store large quantities of logs in the wood yard to ensure a constant supply to the mill throughout the year. In many cases, management of such inventories is limited to processing the logs in chronological order, "first in first out," with no account taken of their origin, harvest period, or moisture content (MC). The moisture content of logs is known to vary widely according to species, logging site, and harvesting season (Gingras and Sotomayor 1992; Linzon 1969; Clark and Gibbs 1957; Gibbs 1939). In addition, logs in storage dry at different rates depending on species, initial moisture content, diameter class, proportion of bark lost during

handling, local weather conditions, and log yard management practices.

For optimum operating conditions, logs entering the mill should have uniform moisture contents. At least, moisture contents should be neither too low nor too high. In the case of OSB mills, large moisture content variations have repercussions on almost all aspects of the manufacturing process, from log conditioning to debarking, flaking, drying, and pressing. They lead to increased production costs and may compromise final product quality. In other wood processing operations (lumber, veneer, pulp, etc.), controlling the moisture content of raw material is also important to ensure process quality control. One way to optimize the management of

log inventories is to have a model capable of predicting log drying rates.

The literature contains only a limited number of studies on this topic, so that little is known on log drying rates. Droessler et al. (1986) conducted a study to assess the rate of weight loss in piled pulpwood and investigated the influence of weather conditions on drying rates. They found that the rate of weight loss in freshly-cut, piled pulpwood was largely constant, but was influenced by environmental conditions such as average daily maximum temperature, average maximum relative humidity, and total rainfall in the days immediately preceding measurement. A model was developed to predict pulpwood weight as a function of time. The model used by Fauchon et al. (2000) to estimate the drying rate of logs during storage takes into account the initial moisture content and the relative humidity of ambient air. The model gives good results for Douglas-fir logs. In addition to climatic conditions, Simpson and Wang (2004) included log diameter in their model, developed to predict air-drying times of debarked logs. Like the models of Droessler et al. (1986) and Fauchon et al. (2000), it gives acceptable results, but remains only applicable to the species considered and to the conditions where data were collected.

Schultz et al. (1997) developed a more advanced model using artificial neural networks. Their model, which accounts for differences in longitudinal and radial moisture content gradients of sprinkled and un-sprinkled bark and wood over time, has proved to be a valuable tool in predicting the moisture content of stored round wood. The sensitivity analysis showed that species, days in storage, and distance from the core had the greatest effects on moisture content measurements, while the effect of drying through log ends on overall log moisture loss was relatively minor. According to the authors, the probable causes for this minor effect were that 1) radial distances from the core to the bark provided a much shorter path for water evaporation than longitudinal travel, and 2) the surface area for radial moisture paths was many times greater than the surface area of log ends. The existence of radial gradients indicated that dry-

ing also occurred through the bark. As pointed out by the authors, this observation ran contrary to the commonly held belief that log drying occurs mostly through the ends. Among the species studied [(*Pinus taeda* (loblolly pine), *Quercus falcata* (southern red oak), *Quercus nigra* (water oak), and *Liquidambar styraciflua* (sweetgum)], loblolly pine maintained higher and more stable moisture contents than sweetgum, water oak, and southern red oak that are hardwood species, which suggested that the role of bark in the stability of a log's moisture content differs according to species.

The objectives of this work were: 1) to develop a finite element model to predict the drying rates of aspen logs during storage on the basis of the water potential concept; and 2) to assess the effects of diameter and length on log drying rates.

MATHEMATICAL MODEL

The model of moisture movement selected for this study is based on the concept of water potential. A detailed description of this concept can be found in Fortin (1979), Cloutier and Fortin (1991), and Zhang and Peralta (1999). It was applied to the prediction of water movement in wood during drying by Cloutier et al. (1992) and Defo et al. (2000). Only the relationships relevant to the present work will be recalled.

From the mass conservation law, we may write:

$$\frac{\partial C}{\partial t} + \vec{\nabla} \cdot \vec{q}_m = 0 \quad (1)$$

where C is the moisture concentration ($\text{kg}_{\text{water}} \text{m}^{-3} \text{moist wood}$); \vec{q}_m is the moisture flux vector ($\text{kg}_{\text{water}} \text{m}^{-2} \text{moist wood s}^{-1}$); and t is the time (s). If we assume thermodynamic equilibrium between water phases in wood and negligible temperature gradients, we can describe the moisture flux with the generalized Darcy's law:

$$\vec{q}_m = -\underline{\underline{K}} \vec{\nabla} \psi \quad (2)$$

where $\underline{\underline{K}}$ is the effective water conductivity tensor ($\text{kg}^2_{\text{water}} \text{m}^{-1} \text{moist wood s}^{-1} \text{J}^{-1}$), function of

moisture content and temperature; ψ is the water potential ($J\ kg^{-1}_{water}$). If we assume that the domain is cylindrical (Fig. 1a) and symmetrical about the longitudinal axis, we can re-write the divergence of the mass flow in a cylindrical coordinates system (r, θ, z) as follows (Potter and Goldberg 1987):

$$\vec{\nabla} \cdot \vec{q}_m = -\frac{1}{r} \left[\frac{1}{\partial r} \left(rK_r \frac{\partial \psi}{\partial r} \right) + \frac{\partial}{\partial \theta} \left(K_\theta \frac{\partial \psi}{\partial \theta} \right) + \frac{\partial}{\partial z} \left(rK_z \frac{\partial \psi}{\partial z} \right) \right] \quad (3)$$

where $K_r, K_\theta,$ and K_z are the radial, angular, and longitudinal components of the water conductivity tensor. Substituting Eq. (3) into Eq. (1) and

assuming that wood is a non-swelling porous medium and that the problem is independent of θ (symmetry about the longitudinal axis z), we obtain the following mass transfer equation:

$$\frac{\partial M}{\partial t} - \frac{100}{G_m \rho_w} \left[\frac{1}{r} \frac{\partial}{\partial r} \left(rK_r \frac{\partial \psi}{\partial r} \right) + \frac{\partial}{\partial z} \left(K_z \frac{\partial \psi}{\partial z} \right) \right] = 0 \quad (4)$$

where G_m is the specific gravity of wood ($kg_{oven-dry\ wood}\ m^{-3}_{moist\ wood}\ kg^{-1}_{water}\ m^3_{water}$); and ρ_w is the density of water ($kg_{water}\ m^{-3}_{water}$). Given the symmetry about the longitudinal axis, the tri-dimensional problem is reduced to a two-dimensional problem in a cylindrical coordinates system, which means that drying occurs only in

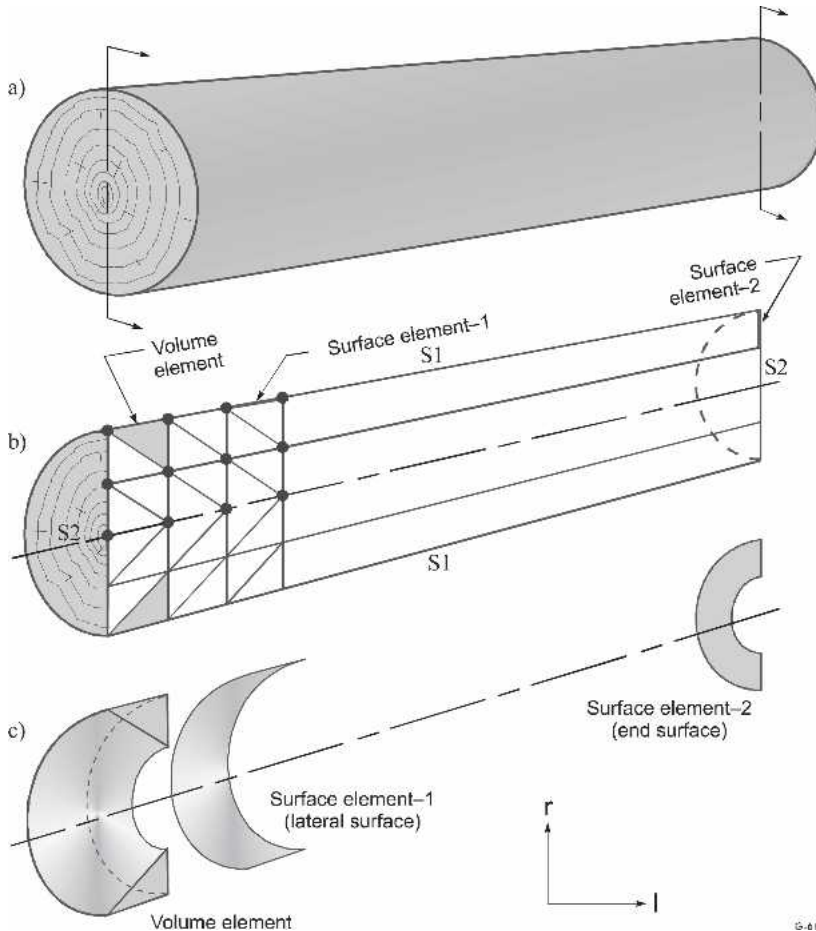


FIG. 1. Meshing of log for numerical resolution: a) physical domain; b) finite element mesh; c) three-nodes triangular linear and two-nodes linear axisymmetric elements.

the radial and longitudinal directions. Equation (4) does not consider the Soret effect, but the effect of the temperature gradient on moisture movement is partially taken into account, as the effective water conductivity and water potential are both dependent on the temperature.

The governing equation for heat transfer includes the change of total enthalpy, the transfer of heat by conduction, and the phase change term:

$$\frac{\partial H}{\partial t} + \vec{\nabla} \cdot \vec{q}_h - \varepsilon(\Delta h_o + \beta \Delta h_s) \frac{\partial C}{\partial t} = 0 \quad (5)$$

where H is the enthalpy of the wood-air-water system (J m^{-3} moist wood); \vec{q}_h is the heat flux vector (J m^{-2} moist wood s^{-1}); ε is the ratio of vapor diffusion to total water movement; Δh_o is the latent heat of vaporization (J kg^{-1} water); Δh_s is the differential heat of sorption (J kg^{-1} water); $\beta = 0$ for M greater than the fiber saturation point (FSP) and $\beta = 1$ for M less or equal than FSP. Heat transfer by conduction is described by Fourier's law:

$$\vec{q}_h = -\underline{k} \vec{\nabla} T \quad (6)$$

where \underline{k} is the thermal conductivity tensor (W m^{-1} moist wood K^{-1}). Using the same assumptions on the physical domain, Eq. (5) can be rewritten in a cylindrical coordinates system:

$$\frac{\partial H}{\partial t} - \left[\frac{1}{r} \frac{\partial}{\partial r} \left(r k_r \frac{\partial T}{\partial r} \right) + \frac{\partial}{\partial z} \left(k_z \frac{\partial T}{\partial z} \right) \right] = Q1 \quad (7)$$

where $Q1 = \varepsilon(\Delta h_o + \beta \Delta h_s) \frac{\partial C}{\partial t}$. Equation (7) does not consider the transfer of heat by convection inside the wood (Dufour effect), which is generally considered negligible.

Initial conditions are given by

$$M(r, z, t = 0) = M_0 \quad (8a)$$

$$\psi(r, z, t = 0) = \psi_0 \quad (8b)$$

$$T(r, z, t = 0) = T_0 \quad (8c)$$

The boundary conditions associated with Eqs. (4) and (7) are:

$$q_m = H_{\psi}(\psi_{wb} - \psi_{\infty}) \text{ on S1} \quad (9a)$$

$$q_m = h_{\psi}(\psi_S - \psi_{\infty}) \text{ on S2} \quad (9b)$$

$$q_h = h_h(T_S - T_{\infty}) + Q2 \text{ on S1 and S2} \quad (9c)$$

where S1 and S2 are radial and end surface boundaries, respectively (Fig. 1b); h_{ψ} is the average mass transfer coefficient ($\text{kg}^2_{\text{water}} \text{m}^{-2} \text{moist wood s}^{-1} \text{J}^{-1}$); ψ_S is the water potential at log end surfaces, ψ_{∞} is the water potential of ambient air, ψ_{wb} is the water potential at the wood/bark interface; h_h is the average heat transfer coefficient ($\text{W m}^{-2} \text{moist wood K}^{-1}$); T_S and T_{∞} are the temperatures at the wood surface and in the medium. The term $Q2$ on the right hand side of Eq. (9c) accounts for the vaporization of water at the log surface: $Q2 = (1 - \varepsilon)(\Delta h_o + \beta \Delta h_s) h_{\psi}(\psi_S - \psi_{\infty})$. H_{ψ} , in Eq. (9a), is the overall mass transfer coefficient, taking into account the resistance of bark to moisture flow. It is estimated from the following relationship, the storage of water in bark or its moisture capacity being considered negligible:

$$H_{\psi} = \frac{1}{R_b + 1/h_{\psi}} \quad (10)$$

where R_b is the resistance of bark to moisture flow ($\text{kg}^{-2}_{\text{water}} \text{m}^2 \text{moist wood s}^1 \text{J}^1$), the ratio of the thickness to the water conductivity of the bark. It is not strictly justified to assume that the water content of the bark is negligible. However, the problem becomes more complex without this analytical restriction, as one would need: 1) to determine the effective water conductivity of bark; and 2) to mesh the bark, thereby increasing unnecessarily the number of elements. The convection coefficients h_{ψ} and h_h can be different for radial and end surfaces, depending on log orientation and wind direction.

FINITE ELEMENT FORMULATION

Using Galerkin's finite element method, Eqs. (4) and (7) have been solved to predict moisture content average and distributions within the log during drying. Temporal discretization was performed on the basis of an Euler implicit scheme. The derivative terms in the weighted residual integrals of Eqs. (4) and (7) were transformed in

the lower-order forms using integration by parts and Gauss's theorem. Details on these transformations in the case of axisymmetric field problems can be found in Ross (1984). The domain under study was discretized in a set of subdomains (Fig. 1b), which in this case are three-node linear axisymmetric triangular elements for domain V and two-node linear axisymmetric elements for the boundary S (Fig. 1c).

APPLICATION TO THE ANALYSIS OF THE INFLUENCE OF DIAMETER AND LENGTH ON DRYING RATES OF ASPEN LOGS

Aspen was selected for this study because it is the species most commonly used in Canada by the OSB industry. After evaluating the resistance of bark to moisture flow and determining model parameters, we applied the model to simulate log drying for different combinations of lengths and diameters.

Material

Twenty-two freshly harvested aspen logs were purchased from a woodland owner from southeastern Quebec, Canada. The logs were 20 to 30 cm in diameter at the butt end, and 2.5 m in length. Two disks, about 2.5 cm thick, were cut at a distance of 20 cm from the ends of each log for the determination of initial moisture contents and specific gravity. Initial moisture contents ranged from 55% to 100% while specific gravity ranged from 0.341 to 0.393.

Drying experiments

Two drying experiments were conducted: one in a laboratory kiln and another under natural conditions. For the kiln-drying test, four logs were selected and cut into two one-meter bolts. The bolts were numbered from 1 to 8, weighed to the nearest kilogram, and then stacked on two rows separated by 19-mm-thick stickers. A fan installed at the top of the kiln produced an air velocity of about 2.5 m/s in the direction perpendicular to the longitudinal axis of the bolts. After a preheating phase at 50°C and 95% RH,

the bolts were allowed to dry at 50°C and 62% RH for 34 days. Each bolt was weighed periodically. This experiment was intended to evaluate the resistance of bark to moisture flow.

For the air-drying test, eight 2-m logs were exposed to outdoor conditions in an open shed to protect them from precipitation. This experiment was intended to confirm the effect of bark on log drying rates. For this purpose, we debarked four of the logs, while the bark on the other four remained intact. In each group, two of the logs were end-coated with a silicone sealant and aluminum foil so that any drying would take place exclusively in the radial direction. We then weighed the logs, stacked them 30 cm off the ground in two courses separated by 38-mm-thick stickers and allowed them to dry for ten months (from November 2001 to September 2002). Each log was weighed periodically.

Determination of model parameters and boundary conditions

To determine the M- ψ relationship and the $K_L(M,T)$ and $K_R(M,T)$ functions, we obtained heartwood and sapwood boards from the remaining logs. For the M- ψ relationship, the specimens were cut to 45 mm \times 10 mm \times 45 mm ($L \times R \times T$), selected, matched, and packed in groups of 12 (six for sapwood and six for heartwood). For the $K_L(M,T)$ and $K_R(M,T)$ functions, the specimens were cut to 45 mm \times 45 mm \times 45 mm ($L \times R \times T$). Six matched groups comprised of six specimens were formed for each combination of wood type (heartwood or sapwood), temperature, and direction of flow, for a total of 72 groups. All the wood specimens were prepared at Forintek Canada Corp.'s Eastern Laboratory and then sent to Université Laval, where they were kept in sealed polyethylene bags and stored at -15°C prior to their use in the experiments. Before each experiment, the specimens were allowed to thaw out for 24 hours over distilled water in closed desiccators held at 21°C.

For the M- ψ relationship, we used the pressure membrane technique for high moisture contents, and equilibration over saturated salt solutions for low moisture contents. These tech-

niques were described in detail in Cloutier and Fortin (1991) and Defo et al. (1999). We took measurements at three temperatures (30°, 45° and 60°C) in the pressure membrane tests, and at two temperatures (30° and 60°C) in the salt solution tests. To determine the $K_L(M,T)$ and $K_R(M,T)$ functions, we used the instantaneous profile method, taking measurements at 30°, 45°, and 60°C, as for the M- ψ relationship. Details on the theoretical background and determination procedure can be found in Cloutier and Fortin (1993). The results obtained are illustrated in Fig. 2 for the M- ψ relationship, and in Fig. 3 for the $K_L(M,T)$ and $K_R(M,T)$ functions. The experimental curves were extrapolated as shown by the broken lines for the M- ψ relationship. In the finite element model, the M- ψ relationship and $K_L(M,T)$ and $K_R(M,T)$ functions are expressed in terms of saturation percentage rather than moisture content, and averaged between heartwood and sapwood.

To assess the effects of diameter and length on log drying rates, we considered only the condition involving air motion perpendicular to the longitudinal log axis. Convective transfer coefficients were estimated for each boundary on the basis of flow geometry. For log ends (S2 boundary, Fig. 1b), we used empirical relations for parallel flow over a flat plate, whereas for radial surface area (S1 boundary, Fig. 1b), we used empirical relations for cross flow over a circular cylinder (Incropera et DeWitt 1996). The mass convection coefficient h_m defined in the empiri-

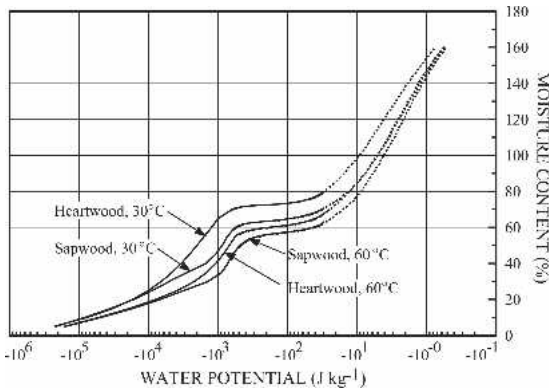


FIG. 2. Moisture content-water potential relationship of aspen wood at 30 and 60°C .

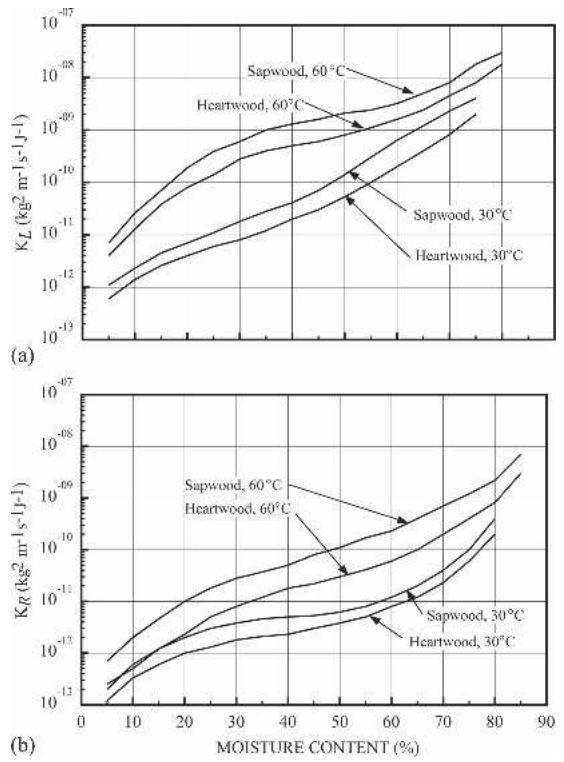


FIG. 3. Effective water conductivity of aspen wood against moisture content at 30 and 60°C: a) longitudinal direction; b) radial direction.

cal relations is based on the concentration of water vapor in the air. Thus, the mass convection coefficient h_ψ , based on the water potential, needs to be expressed from h_m :

$$h_\psi = h_m \frac{CA_S - CA_\infty}{\psi_S - \psi_\infty} \quad (11)$$

where CA_S is the concentration of water vapor in the air in equilibrium with the wood surface ($kg_{water} m^{-3}_{air}$); and CA_∞ is the concentration of water vapor in ambient air ($kg_{water} m^{-3}_{air}$).

It is difficult to determine the water conductivity of bark, as it is relatively thin. We therefore resorted to a trial and error approach to find an appropriate value for parameter Rb in Eq. (10). The predicted drying curves based on different Rb values are shown in Fig. 4 with experimental data obtained for bolts No. 5 and No. 7 during artificial drying. The butt diameters

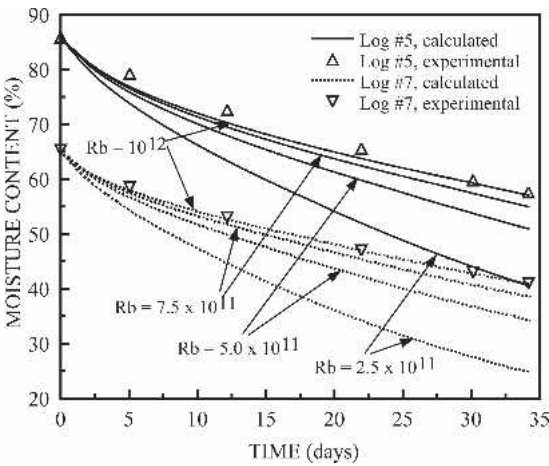


FIG. 4. Experimental drying curves of aspen logs dried at 50°C and calculated drying curves obtained with different values of bark resistance Rb.

were 0.030 m and 0.023 m for bolts No. 5 and No. 7, respectively. The numerical solutions obtained with Rb equal to 10^{12} are in satisfactory agreement with experimental data. If bark thickness is 0.01 m, the water conductivity of bark corresponding to an Rb value of 10^{12} is roughly 10^{-14} , which can be considered an average, as it is known to vary with moisture content and temperature for wood.

Tremblay et al. (1999) determined experimentally the ratio of vapor diffusion to total water movement, ϵ , in the case of red pine sapwood in the radial direction at 18°, 56°, and 85°C. Their experimental results showed that ϵ increased from 0.15 to 0.5 as moisture content decreased from values close to saturation to about 15%, while temperature had no significant effect on ϵ . We used these results in our code, assuming that ϵ is not species-dependent. As for ϵ , the thermal conductivity and other parameters were deduced from the literature.

RESULTS AND DISCUSSION

Impact of bark on aspen logs drying rate

Drying curves obtained for logs dried under natural conditions were difficult to analyze, as surface checking and end-splitting appeared rap-

idly on debarked logs, leading to excessive drying (Fig. 5). Consequently, we were unable to compare the drying rate of logs with and without bark. However, the results show that the logs with full bark coverage and sealed ends did dry, albeit more slowly (average drying rate from April to August = 0.08%/day) than those with unsealed ends (0.14%/day). This confirms that logs also lose moisture through the bark, as pointed out by Schultz et al. (1997). Despite checking and splitting, the excessive drying rate of debarked logs indicates that bark slows down the drying process. As stated by Meyer et al. (1981), impermeable periderm layers in the bark slow down moisture movement from the wood to the surrounding atmosphere.

Influence of length and diameter on log drying rate

The characteristics of the logs used for the analysis of dimensional effects on log drying rate are listed in Table 1. The logs considered were 1.22, 2.44, 4.88, and 14.40 m in length, with butt end diameters ranging from 15.2 cm to 55.9 cm. Each log was identified by its length and butt end diameter. For example, L01D15 identified a log that was 1.22 m in length and 15.2 cm in butt end diameter. In the OSB industry, raw material is normally stored in log form (2.44 m) or in full tree lengths (14.4-m average length). The small end diameters of 2.44- and

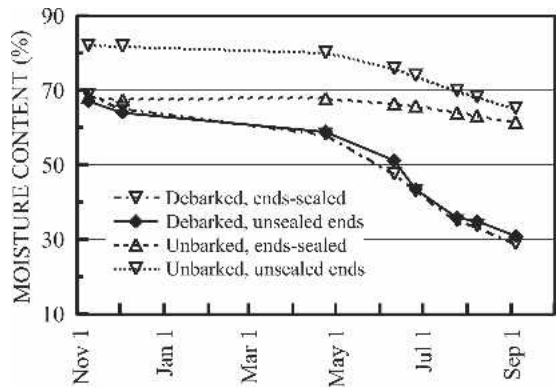


FIG. 5. Drying curve of aspen logs dried under natural conditions.

TABLE 1. Characteristics of logs used for the analyses of dimensional effects on the log drying rate.

Identification	Length (m)	Diameter		Identification	Length (m)	Diameter	
		Large (cm)	Small (cm)			Large (cm)	Small (cm)
L01D15	1.22	15.2	14.3	L04D15	4.88	15.2	12.6
L01D20	1.22	20.3	18.8	L04D20	4.88	20.3	16.2
L01D25	1.22	25.4	23.4	L04D25	4.88	25.4	20.2
L01D30	1.22	30.5	27.9	L04D30	4.88	30.5	22.6
L01D35	1.22	35.6	32.6	L04D35	4.88	35.6	26.0
L01D40	1.22	40.6	37.1	L04D40	4.88	40.6	29.3
L01D45	1.22	45.7	41.7	L04D45	4.88	45.7	33.4
L01D50	1.22	50.8	46.3	L04D50	4.88	50.8	37.2
L01D55	1.22	55.9	50.9	L04D55	4.88	55.9	40.9
L02D15	2.44	15.2	13.9	L14D15	14.4	15.2	10.1
L02D20	2.44	20.3	18.3	L14D20	14.4	20.3	11.8
L02D25	2.44	25.4	23.5	L14D25	14.4	25.4	13.5
L02D30	2.44	30.5	26.3	L14D30	14.4	30.5	15.2
L02D35	2.44	35.6	30.5	L14D35	14.4	35.6	16.9
L02D40	2.44	40.6	34.5	L14D40	14.4	40.6	18.7
L02D45	2.44	45.7	38.9	L14D45	14.4	45.7	22.2
L02D50	2.44	50.8	43.3	L14D50	14.4	50.8	25.2
L02D55	2.44	55.9	47.7	L14D55	14.4	55.9	27.2

14.40-m logs were obtained from field measurements, whereas those of 1.22- and 4.88-m logs were interpolated. Initial moisture content and temperature conditions for the whole domain were set to 100% and 15 °C, respectively. The parameters used were: $T_{\infty} = 24^{\circ}\text{C}$; $\text{RH} = 70\%$; wind speed = 2.5 m/s. The wind direction was chosen so as to simulate log drying rate with air motion perpendicular to the log’s longitudinal axis. With these conditions, we simulated 60 days of seasoning.

Figure 6 shows average drying rate over a

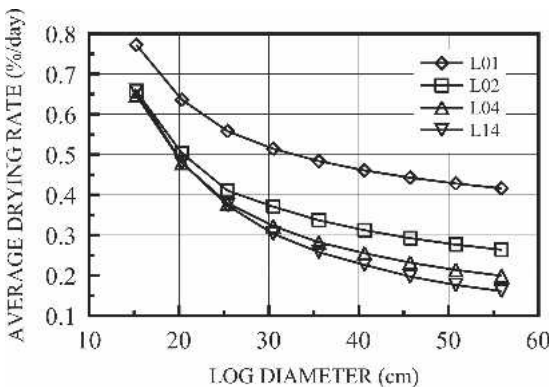


FIG. 6. Influence of log diameter on the average drying rate in the case of a 2D drying.

60-day period as a function of log diameter and length. For these simulations, logs were allowed to dry simultaneously in the radial and longitudinal directions. It is clear that small-diameter logs dried faster than larger ones. As diameter increased, the average drying rate decreased for all lengths. As can be observed, however, the effect of diameter on average drying rate was marginal in the case of the larger logs. Log length also affected drying rate, as shown in Fig. 7 where average drying rates have been plotted against length for some of the diameter classes. In all diameter classes, shorter logs dried faster than longer ones. The effect of length on

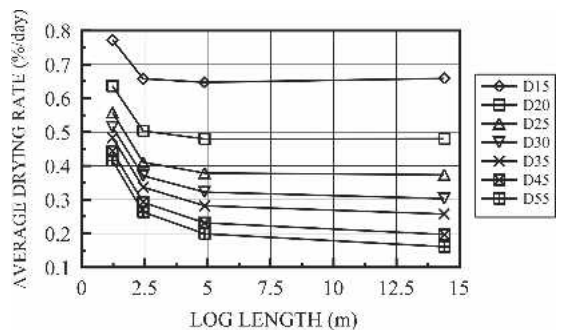


FIG. 7. Influence of log length on the average drying rate in the case of a 2D drying.

average drying rate was more pronounced in the shorter logs, while it was marginal in lengths greater than 5 m. This is due to the path of the moisture flow in the longitudinal direction becoming increasingly long as log length increases, with the result that less moisture reaches end surfaces. This may be seen more clearly in Fig. 8, which shows two-dimensional moisture content distributions at the end of simulation for the D25 diameter class and length groups L01, L04, and L14. Drying through log ends was limited to a relatively small distance from the ends of long logs because moisture had to cover a longer distance than in short logs (Figs. 8b and 8c). Due to tapering, the small end of long log dries faster than the butt end, but essentially in the radial direction (Fig. 8 c).

In order to better understand the effects of log dimensions on drying rate, we simulated one-dimensional drying (radial and longitudinal), un-

der the same conditions as used for two-dimensional simulations. To this end, we set moisture flux to zero on the S2 boundary for radial drying, and the S1 boundary for longitudinal drying. Table 2 presents average drying rates in the case of two-dimensional (2D), radial (R), and longitudinal (L) drying, together with the ratio of the average drying rate in a given direction to that of total 2D drying. The combined percentages of moisture loss in the radial

TABLE 2. Average drying rate (ADR) for two-dimensional (2D) and one-dimensional (R and L) drying and the corresponding percentage of moisture loss.

Log	2D		R		L	
	ADR (%/day)	Ratio ^a (%)	ADR (%/day)	Ratio (%)	ADR (%/day)	Ratio (%)
L01D15	0.773	100	0.469	60.8	0.338	43.7
L01D20	0.636	100	0.310	48.7	0.334	52.5
L01D25	0.558	100	0.221	39.6	0.330	59.2
L01D30	0.514	100	0.167	32.5	0.328	63.7
L01D35	0.484	100	0.143	29.5	0.326	67.3
L01D40	0.461	100	0.119	25.9	0.323	70.1
L01D45	0.443	100	0.101	22.9	0.321	72.4
L01D50	0.428	100	0.088	20.6	0.318	74.2
L01D55	0.416	100	0.079	19.0	0.316	75.9
L02D15	0.658	100	0.477	72.6	0.170	25.8
L02D20	0.504	100	0.316	62.7	0.168	33.3
L02D25	0.411	100	0.221	53.9	0.165	40.3
L02D30	0.371	100	0.173	46.7	0.164	44.2
L02D35	0.337	100	0.149	44.2	0.163	48.3
L02D40	0.312	100	0.124	39.8	0.162	51.7
L02D45	0.293	100	0.108	36.8	0.160	54.8
L02D50	0.277	100	0.093	33.4	0.159	57.3
L02D55	0.264	100	0.082	31.0	0.158	59.7
L04D15	0.647	100	0.516	79.8	0.088	13.5
L04D20	0.480	100	0.348	72.5	0.087	18.1
L04D25	0.379	100	0.250	65.9	0.086	22.6
L04D30	0.323	100	0.199	61.8	0.085	26.5
D04D35	0.282	100	0.154	61.8	0.085	30.0
L04D40	0.255	100	0.138	54.2	0.084	33.0
L04D45	0.232	100	0.116	50.3	0.083	35.9
L04D50	0.214	100	0.102	47.8	0.082	38.5
L04D55	0.199	100	0.089	44.8	0.082	41.0
L14D15	0.659	100	0.619	94.1	0.031	4.7
L14D20	0.480	100	0.409	85.2	0.031	6.4
L14D25	0.374	100	0.310	83.0	0.031	8.2
L14D30	0.303	100	0.248	81.8	0.031	10.1
L14D35	0.258	100	0.202	78.5	0.031	11.8
D14D40	0.226	100	0.172	76.3	0.031	13.5
L14D45	0.197	100	0.143	72.6	0.030	15.1
L14D50	0.176	100	0.122	69.4	0.029	16.7
L14D55	0.161	100	0.105	65.2	0.029	18.2

^a: Ratio of the average drying rate to that of the 2D drying.

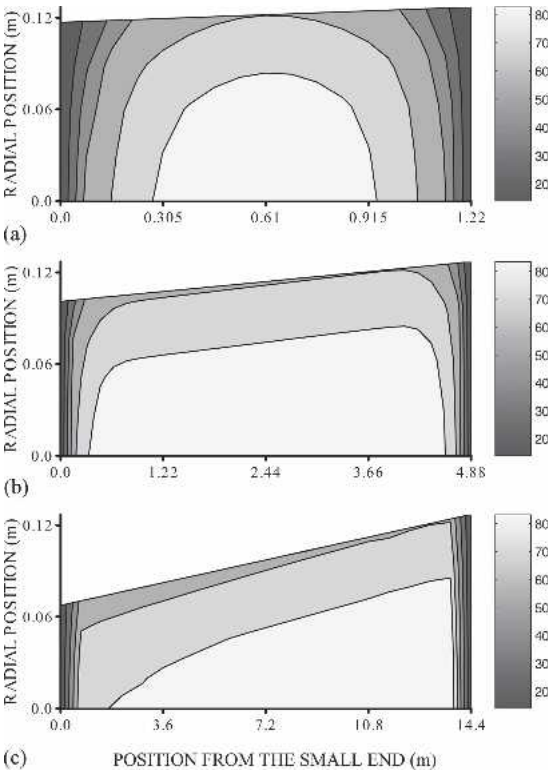


FIG. 8. Two-dimensional M distributions at the end of simulation for lengths L01 (a), L04 (b) and L14 (c) and diameter D25, in the case of a 2D drying.

and longitudinal directions added up to less than 100% in all logs except L01D15 and L01D20, where it reached 104.5% and 101.3% respectively. These differences may be explained by the fact that, during two-dimensional drying, moisture is subjected to two driving forces, with interactions between moisture fluxes in the radial and longitudinal directions. Thus, the ratio presented in Table 2 may be slightly different from the actual moisture loss occurring in a given direction when drying occurs simultaneously in the radial and longitudinal directions, but the trend would be essentially the same.

When the logs were subjected to one-dimensional drying in radial direction, the average drying rate in all length groups was highest in small-diameter logs, and gradually diminished as diameters increased. The length effect is minimal for each diameter class as shown in Table 2. For example, drying rates were 0.469%, 0.477%, 0.516%, and 0.619%/day for logs L01D15, L02D15, L04D15, and L14D15, respectively. This is ascribed to the substantial decrease in diameter from the butt end to the small end. In a perfectly cylindrical log, there would be no length effect when the log is subjected to radial drying only.

When the logs were subjected to one-dimensional drying in longitudinal direction, the average drying rate decreased with increase in length as revealed in Table 2 for a given diameter class. For example, it varied from 43.7%/day for L01 to 4.7%/day for L14 in the case of D15. For each length group, there was no diameter effect on the average drying rate. The small variations observed for each length group were expected, due to the empirical relations used to calculate the average mass transfer coefficient; which is inversely proportional to the characteristic length.

The ratio of moisture loss in radial drying was 60.8% for L01D15, and decreased gradually when diameter increased, down to 19.0% for L01D55. In the same length group, the ratio of moisture loss in longitudinal drying was 43.7% for D15, and it increased with increasing diameter, reaching 75.9% for D55. The same trend was observed in length groups L02, L04, and

L14. However, when the length increased, the percentage of moisture loss in the radial direction increased. In the D15 diameter class, for example, the ratio of radial drying stood at 60.8%, 72.6%, 79.8%, and 94.1% respectively for length groups L01, L02, L04 and L14, while the ratios of longitudinal drying decreased from 43.7% to 25.8%, 13.5%, and 4.7% for the same lengths.

We therefore concluded that, for a given log length, the ratio of radial drying decreased when the diameter increased. At the same time, longitudinal drying became increasingly significant as diameter increased. In a given diameter class, radial drying increased and longitudinal drying decreased as length increased. In the particular case of long logs (L14), most moisture loss occurred in the radial direction (94.1% and 65.2% respectively in the D15 and D55 diameter classes), despite the resistance of bark to moisture flow. This may be attributed to the fact that radial distances from the core to the bark provide a much shorter path than longitudinal distances and that the lateral surface area available for moisture evaporation is many times greater than the surface area of log ends.

Effective water conductivity varies with the structural direction as shown in Fig. 3. At 30°C, the ratio of longitudinal to radial conductivity (K_L/K_R) varies from 2 (at lower moisture content levels) to 30 (at higher levels). Thus, the orthotropy of wood regarding effective water conductivity, the resistance of bark to moisture flow, and the ratio of log length to diameter would explain the behavior observed at relatively high moisture contents. Consequently, the results observed in this study of aspen logs could be different with 1) logs of the same species at lower moisture contents, due to the nature of the moisture flow, which is diffusive, and the lower K_L/K_R ratio; and 2) logs of other species, since water conductivity and the K_L/K_R ratio vary from one species to another. The resistance of bark to moisture flow probably varies as well, as pointed out by Schultz et al. (1997); according to their study on loblolly pine, southern red oak, water oak, and sweetgum, drying at log ends was not a significant factor in overall moisture loss in

the case of 1.52-m-long bolts and diameters ranging from 12.7 cm to 21.59 cm. The presence or absence of juvenile wood and the ratio of heartwood to sapwood (not considered in this study) can also affect the drying pattern observed.

All three situations considered above (i.e. two-dimensional drying, one-dimensional drying in radial or longitudinal direction) may be encountered in the same wood yard. In a large log pile subjected to a wind direction perpendicular to the longitudinal log axis, the wind probably does not penetrate inside the pile. Thus, the logs located in the core of the pile and, to some extent, those at the bottom of the pile may be limited to longitudinal drying. In this case, the drying rate is similar for all diameter classes, and sorting the logs according to diameter classes would be useless. Two-dimensional drying may occur in logs located at the top or the sides of the pile and would also apply to a pile consisting of short logs subjected to an air flow parallel to the longitudinal direction of the logs. When logs are stored in three or more piles placed one close to another or end to end, logs from the center piles may dry only in the radial direction, as the absence of gaps between the piles restricts air flow along end surfaces. In such cases, log sorting could be considered as a means to promote moisture content uniformity in the logs being fed to the mill.

CONCLUSIONS

The mathematical model presented in this paper describes heat and mass transfer in logs during the drying process. The model was developed on the basis of a macroscopic approach known as the water potential concept. The moisture content-water potential relationship and effective water conductivity were determined from independent experiments, and the resistance of bark to the flow of moisture was estimated by fitting experimental drying curves to theoretical ones. To solve the system of nonlinear partial differential equations, we used the finite element method. After validation, the model was applied

to simulate the effect of length and diameter on aspen log drying rate.

With a bark resistance of 10^{12} , the drying curve obtained with the model was in agreement with the experimental data. The simulation of two- and one-dimensional drying shows that the diameter and length have a strong effect on the log drying rate. Small-diameter logs dry faster than large ones. Short logs dry faster than long ones. However, beyond a critical diameter or length, there is no marked difference in drying rates for large or long logs. With the exception of long logs where the drying occurs essentially in radial direction, radial drying is predominant in small-diameter logs whereas for large logs, longitudinal drying is predominant.

ACKNOWLEDGMENTS

This project has been supported financially by the Natural Sciences and Engineering Research Council of Canada (NSERC) through its IRF program and by Forintek members through its National Research Program.

REFERENCES

- CLARK, J., AND R. D. GIBBS. 1957. Further investigations of seasonal changes in moisture contents of certain Canadian forest trees. *Can. J. Botany*. 35:219–253.
- CLOUTIER, A., AND Y. FORTIN. 1991. Moisture content-water potential relationship of wood from saturated to dry conditions. *Wood Sci. Technol.* 25(4):263–280.
- , AND ———. 1993. A model of moisture movement in wood based on water potential and the determination of the effective water conductivity. *Wood Sci. Technol.* 27(2):95–114.
- , ———, AND G. DHATT. 1992. A wood drying finite element model based on the water potential concept. *Drying Technol.* 10(5):1151–1181.
- DEFO, M., Y. FORTIN, AND A. CLOUTIER. 1999. Moisture content-water potential relationship of sugar maple and white spruce wood from green to dry conditions. *Wood Fiber Sci.* 31(1):62–70.
- , A. CLOUTIER, AND Y. FORTIN. 2000. Modeling vacuum-contact drying of wood: The water potential approach. *Drying Technol.* 18(8):1737–1778.
- DROESSLER, T., J. L. BOWYER, T. BURK, E. JAMROCK, AND R. ANTILLA. 1986. Rate of weight loss in piled pulpwood. Station Bulletin AD-Sb-3036. Ag. Exp. Station. Univ. Minnesota, MN, 18 pp.
- FAUCHON, T., G. CHANTRE, AND C. DELEUZE. 2000. How to

- control the variation of the wood moisture content of logs from the stand to the woodyard? The contribution of both direct techniques of assessment and modelling. Pages 65–81 in 3rd Workshop on Measuring of Wood Properties, Grades and Qualities in the Conversion Chains and Global Wood Chain Optimization. Espoo, Finland.
- FORTIN, Y. 1979. Moisture content–matric potential relationship and water flow properties of wood at high moisture contents. Ph.D. thesis, Univ. of British Columbia, Vancouver, BC. Canada. 187 pp.
- GIBBS, R. D. 1939. Studies in tree physiology. I. General introduction. Water contents of certain Canadian trees. *Can. J. Research.* 17: 460–482.
- GINGRAS, J.-F., AND J. SOTOMAYOR. 1992. Wood moisture variation in woodlands inventory: A case study. Wood Harvesting Technical Note TN-192. FERIC, Canada. 6 pp.
- INCROPERA, F. P., AND D. P. DEWITT. 1996. Fundamentals of heat and mass transfer, 4th ed., John Wiley and Sons, New York, NY. 886 pp.
- LINZON, S. N. 1969. Seasonal water content and distribution in eastern white pine. *Forestry Chron.* 45(1): 38–43.
- MEYER, R. W., R. M. KELLOG, AND W. G. WARREN. 1981. Relative density, equilibrium moisture content, and dimensional stability of western hemlock bark. *Wood Fiber.* 13(2): 86–96.
- POTTER, M.C., AND J. GOLDBERG. 1987. Mathematical methods. 2nd Ed. Prentice Hall, Englewood Cliffs, NJ. 639 pp.
- ROSS, C.T.F. 1984. Finite element programs for axisymmetric problems in engineering. Ellis Horwood Limited, West Sussex, England. 297 pp.
- SCHULTZ, E. B., T. G. MATNEY, AND W. F. WATSON. 1997. Prediction of moisture contents for sprinkled and unsprinkled stacked roundwood over time. Pages 289–299 in TAPPI Pulping Conference, San Francisco, CA.
- SIMPSON, W. T., AND X. WANG. 2004. Estimating air-drying times of small-diameter ponderosa pine and Douglas-fir logs. *Forest Prod. J.* 54(12):24–28.
- TREMBLAY, C., A. CLOUTIER, AND B. GRANDJEAN. 1999. Experimental determination of the ratio ε of moisture movement in the vapor phase over total moisture movement in wood during a drying session. *Wood Fiber Sci.* 31(3): 235–248.
- ZHANG, J., AND P. N. PERALTA. 1999. Moisture content-water potential characteristic curves for red oak and loblolly pine. *Wood Fiber Sci.* 31(4):360–369.